

1 **Fire-precipitation interactions amplify the quasi-biennial
2 variability of fires over southern Mexico and Central America**

3 Yawen Liu ^{1,2}, Yun Qian ^{3*}, Philip J. Rasch ^{3*}, Kai Zhang ³, L. Ruby Leung³, Yuhang Wang ⁴,
4 Minghuai Wang ^{1,2}, Hailong Wang ³, Xin Huang^{1,2}, and Xiu-Qun Yang ¹

5 ¹School of Atmospheric Sciences, Nanjing University, China

6 ²Joint International Research Laboratory of Atmospheric and Earth System Sciences & Institute
7 for Climate and Global Change Research, Nanjing University, China

8 ³Pacific Northwest National Laboratory, Richland, Washington, USA

9 ⁴School of Earth and Atmospheric Sciences, Georgia Institute of Technology, Atlanta, Georgia,
10 USA

11 *Correspondence to:* Yun Qian and Philip J Rasch and (yun.qian@pnnl.gov and
12 Philip.Rasch@pnnl.gov)

13 **Abstract.** Fires have great ecological, social, and economic impacts. However, fire prediction and
14 management remain a challenge due to a limited understanding of their role in the Earth system.
15 Fires over southern Mexico and Central America (SMCA) are a good example, which greatly
16 impact local air quality and regional climate. Here we report that the spring-peak (Apr-May) fire
17 activities in this region have a distinct quasi-biennial signal based on multiple satellite datasets
18 measuring different fire characteristics. The variability is initially driven by the quasi-biennial
19 variations of precipitation. Composite analysis indicates that strong fire years correspond to
20 suppressed ascending motions and weakened precipitation over the SMCA. The anomalous
21 precipitation over the SMCA is further found to be mostly related to the East Pacific-North Pacific
22 (EP-NP) pattern two months previous to the fire season. The positive phase of EP-NP leads to
23 enhanced precipitation over the eastern US yet suppressed precipitation over SMCA, similar to the
24 spatial pattern of precipitation difference between strong and weak fire years. Meanwhile, the
25 quasi-biennial signals in precipitation and fires appear to be amplified by their interactions through
26 a positive feedback loop on short timescales. Model simulations show that in strong fire years,
27 more aerosol particles are released and transported downstream over the Gulf of Mexico and the
28 eastern US, where suspended light-absorbing aerosols warm the atmosphere and cause ascending
29 motions of the air aloft. Subsequently, a compensating downward motion is formed over the fire
30 source region and ultimately suppresses precipitation and intensifies fires. Statistical analysis
31 shows the different duration of the two-way interaction, where the fire suppression effect by
32 precipitation lasts for more than 20 days, while fire leads to a decrease in precipitation at shorter
33 time scales (3-5 days). This study demonstrates the importance of fire-climate interactions in
34 shaping the fire activities on interannual scale and highlights how precipitation-fire interactions at
35 short timescales contribute to the interannual variability of both fire and precipitation.

36 **1 Introduction**

37 Natural and human-induced fires are key features of the Earth system (Bowman et al., 2009).
38 Uncontrolled large fires damage biodiversity, affect human health, and incur high economic costs
39 (Knorr et al., 2017; Aguilera et al., 2021; Bowman et al., 2017). Comprehensive knowledge of
40 fires' causes, variability, and climate effects is necessary to accommodate or manage fires
41 effectively, and to mitigate adverse societal impacts.

42 Changes in climate alter fire regimes (Power et al., 2008; Jolly et al., 2015), because the occurrence
43 and intensity of fires depend on meteorological factors such as precipitation, wind, and humidity
44 (Flannigan et al., 2009; Marlon et al., 2008; Abram et al., 2021; Fang et al., 2021). Fires alter
45 weather and climate as well: they are important sources of aerosol particles that modify Earth's
46 energy and water budget either by directly absorbing and scattering sunlight or affecting cloud
47 microphysical processes (Voulgarakis and Field, 2015; Jiang et al., 2020; Liu et al., 2018; Yue et
48 al., 2022; Lu et al., 2018). There are many modes of interaction. The modes are complex, operate
49 through a variety of mechanisms, and manifest on a large variety of time and space scales (Ding
50 et al., 2021; Zhang et al., 2022). For example, Huang et al. (2023) have demonstrated that synoptic-
51 scale fire-weather feedback plays a prime role in driving extreme fires in the Mediterranean and
52 monsoon climate regimes over the US West Coast and Southeastern Asia. On interannual scales,
53 fires in the maritime subcontinent have been shown to affect SSTs, land temperature as well as
54 atmospheric stability, and influence ENSO on 3-6 year timescales (Tosca et al., 2010). The
55 extreme 2019-2020 Australian fires have also been demonstrated to contribute to the 2020-2022
56 strong La Niña event by enhancing cloud albedo, cooling and drying out the air, and forming a
57 positive feedback between the northward migration of intertropical convergence zone and sea
58 surface temperature cooling in the Niño3.4 region (Fasullo et al., 2023). Moreover, on even longer
59 timescales, fires can affect the accumulation of carbon dioxide and methane by modifying global
60 features like the Hadley circulation that change precipitation and temperature patterns and
61 eventually affect forest ecosystems to produce feedback operating over decades and centuries
62 (Crutzen and Andreae, 1990; Page et al., 2002; Tosca et al., 2013). It is hence necessary to explore
63 fire characteristics with special considerations of their multi-scale variability and feedback.

64 From a global perspective, fires occur progressively more frequently towards the tropics (Mouillet
65 and Field, 2005). Tropical savanna and forest burning contribute approximately 80% of global

66 open fire emissions (Bond et al., 2013). However, tropical regions also feature a great diversity of
67 climate-weather systems that affect fire occurrence and seasonality. In the tropical Northern
68 Hemisphere, fires over tropical southern Mexico and Central America (SMCA) occur during the
69 Feb-May dry season and peak in April-May (Magi et al., 2012). These fire activities have a
70 substantial influence on local air quality and human health (e.g., over Mexico City [19-20° N, 98-
71 100°W] and the Yucatan region (Crounse et al., 2009; Yokelson et al., 2007; Yokelson et al.,
72 2009). Fire emissions over the SMCA region also affect the eastern US after long-range transport
73 (Kreidenweis et al., 2001; Lee et al., 2006; Rogers and Bowman, 2001). Understanding the
74 processes that shape fire variabilities over this region is hence important locally (for air quality
75 and fire management) and over broader regions.

76 Here, for the first time, we report a distinct quasi-biennial variability of fire activities over the
77 southern Mexico and Central America region (SMCA, 10-25°N, 80-100°W) during the peak
78 burning months (April – May) over 2003-2019 by validating different fire characteristics~~s~~ with the
79 use of multiple independent datasets. We further explored~~d~~ the dominant causes of this quasi-
80 biennial signal and provided~~d~~ concrete evidence for positive fire-precipitation feedback on short
81 timescales to amplify the quasi-biennial signal based on model simulations.

82 **2 Data and Methods**

83 **2.1 Observations**

84 Two sets of fire emission inventories were used to investigate the interannual variability of fire
85 activities. The Global Fire Emissions Database with small fires version 4.1 (GFED v4.1s) is a
86 bottom-up inventory that generates fire-consumed dry matter using fire-burned areas combined
87 with emission factors (Giglio et al., 2013; Randerson et al., 2012). GFED v4.1s provides monthly
88 mean fire-consumed dry matter in total and for individual fire types at 0.25-degree spatial
89 resolution. The Quick Fire Emissions Dataset (QFED) is a top-down emission inventory that
90 generates fire emissions by using empirical relationships between fire-consumed dry matter
91 consumption and fire radiative power (Koster et al., 2015). Daily emissions of fire-emitted species
92 at 0.1 horizontal resolution from QFED version 2.5 were examined. Since the interannual
93 variations of different species are consistent, only variation of fire-emitted black carbon (BC) is
94 shown here. We focused on the fire activities after 2003 to exclude the influence of the extremely

95 strong ENSO events, specifically the 1997/1998 El Niño event and the subsequent 1998-2000 La
96 Niña event, which are among the most powerful ENSO events in recorded history.

97 We also examined the interannual variation of fire-induced changes in aerosol optical depth based
98 on the MERRA-2 reanalysis data (Gelaro et al., 2017) and Level 3 version 4.2 CALIPSO satellite
99 dataset (Winker et al., 2013). For the MERRA-2 data, monthly mean BC aerosol optical depth
100 (AOD) was used for a better comparison with the BC emission from QFED emission data. The
101 CALIPSO product divides aerosol into six sub-types, and the gridded monthly mean 532nm AOD
102 for the biomass burning aerosol type under all-sky conditions was analyzed. We used the MODIS
103 version 6.1 gross primary productivity (GPP) product (MOD17A2H, (Running, 2021)), which
104 measures the growth of the terrestrial vegetation NOAA Climate Data Record of Advanced Very
105 High Resolution Radiometer (AVHRR) version 5 leaf area index (LAI) (Vermote, 2019), which
106 is defined as the one-sided green leaf area per unit ground surface as a proxy for fuel load. A
107 cumulative 8-day composite of Daily LAI GPP values product is provided with a 500m pixel size.
108 on a 0.05-degree grid. The average of GPP in the month (March) LAI in the 10 days previous prior
109 to the burning season is examined.

110 In order to investigate the climate influence on fire activities, we analyzed monthly mean
111 temperature and maximum temperature from the Climatic Research Unit gridded Time Series
112 (CRU TS) version 4.06 (Harris et al., 2014). The dataset is constructed based on station
113 observations and provides monthly data over the global land surface at 0.5-degree resolution. Apart
114 from the CRU dataset, two sets of satellite observations of precipitation were analyzed: the
115 monthly Integrated Multi-satellitE Retrievals for GPM (IMERG) precipitation estimates at 0.1
116 degrees (Huffman et al., 2015) and the 1-degree daily (version 1.3), 2.5-degree monthly
117 (version2.3) Global Precipitation Climatology Project (GPCP) precipitation estimates (Adler et al.,
118 2018; Adler, 2017). IMERG is intended to intercalibrate and merge satellite microwave
119 precipitation estimates together with microwave-calibrated infrared satellite estimates and
120 precipitation gauge analyses (Huffman et al., 2020). Monthly mean 500hPa vertical velocity (ω)
121 at 2.5 degrees from NCEP/NCAR reanalysis (Kanamitsu et al., 2002) and 10m wind speed at 0.25
122 degrees from ERA5 reanalysis (Hersbach et al., 2020) were also used in our work. In order to
123 understand the interannual variation of precipitation, we examined the relationship between
124 precipitation and ten different teleconnection patterns, including Atlantic Meridional Mode

125 (AMM), East Pacific/North Pacific Oscillation (EP/NP), ENSO, North Atlantic Oscillation
126 (NAO), North Tropical Atlantic index (NTA), Pacific North American index (PNA), Tropical
127 Northern Atlantic index (TNA), Tropical Southern Atlantic index (TSA), Western Hemisphere
128 warming pool (WHWP), Quasi-biennial Oscillation (QBO). These indice and their detailed
129 definitions can be obtained from <https://psl.noaa.gov/data/climateindices/list/>.

130 **2.2 Model experiment**

131 The CESM2.1.0 model with the Community Atmosphere Model version 6 (CAM6) (Danabasoglu
132 et al., 2020) was used to investigate the feedback of fire-emitted aerosols on precipitation. The
133 F2000 component set was used with the prescribed sea surface temperature in the year 2000. The
134 horizontal resolution is set as 0.9-degree latitude by 1.25-degree longitude with 32 vertical levels.
135 Two groups of simulations were conducted. Each was driven by the representative fire emissions
136 in strong and weak fire years and referred to as Case_Strong and Case_Weak. The difference in
137 variables (e.g., temperature and precipitation) between the two cases (Case_Strong minus
138 Case_Weak) indicate the influence, or difference in feedback, caused by stronger fire emissions.
139 As our work focused on the influence of fire activities over SMCA, only fire emissions over the
140 SMCA region were considered. Since fire emissions and anthropogenic emissions are specified
141 separately in the CESM2 model, we modified ~~T~~the default fire emission inventory (Van Marle et
142 al., 2017) in CESM2.1.0 ~~was modified~~ accordingly while global anthropogenic emissions ~~were~~
143 kept unchanged and remained the same between cases. Given that composite analysis indicates
144 fire emissions in weak fire years are approximately half those in strong fire years. We simply used
145 the average of fire emissions during strong fire years in Case_Strong, and reduced these by half in
146 Case_Weak. More subtle changes in fire locations between strong and weak fire years are hence
147 ignored. Furthermore, global climate models have long been found to underestimate fire-induced
148 changes in aerosols (Zhong et al., 2022). Hence, in order to ensure the simulated difference in fire-
149 induced AOD between Case_Strong and Case_Weak is comparable to observations, the default
150 inventory is multiplied by a factor of 3 to ensure the simulated fire-induced AOD changes are
151 comparable to observations. For each group, 9 ensemble simulations were performed with slight
152 differences in their initial conditions. The ensemble mean is calculated as the average of 9
153 members. All simulations start on Jan.1 with a 3-month spin-up time. The T-test is used to identify
154 statistically significant differences between Case_Strong and Case_Weak.

155 **3 Results**

156 **3.1 Biennial variability of fire activities**

157 We focus on the southern Mexico and Central America region (SMCA) covering both the Yucatan
158 region and Mexico City. Major fire types in this region consist of deforestation fires, savanna fires,
159 and agricultural waste burning, which respectively are estimated to consume 45.5%, 42.1%, and
160 12.40% of the total burned dry matter during the peak burning months (Apr-May) of the 17-year
161 (2003-2019) study period.

162 As shown in Fig. 1a, GFEDv4.1s estimates of the regional sum of the total dry matter consumed
163 by fire activities feature obvious quasi-biennial variability. Generally speaking, fire activities in
164 odd-numbered years show higher consumption of dry matter than adjacent even-numbered years
165 with the only exception of the year 2016, which might be related to a long-lasting El Niño event
166 spanning 2014-2016. Composites of fire consumption of dry matter indicate enhanced fire
167 activities along both sides of the high terrains in odd-numbered years, and the most profound
168 difference appears over the bordering area between southern Mexico and Guatemala (Fig. S24).
169 The average fire-consumed dry matter here differs by more than a factor of 6 between odd-
170 numbered and even-numbered years.

171 The quasi-biennial variability of fire activities is also evident when examining fire emissions of
172 typical fire-emitted species based on the QFED inventory (Fig. 1b). Similarly, fire-emitted BC in
173 odd-numbered years is basically higher than those in the adjacent even-numbered years, when
174 considering both regional mean and medium values. Furthermore, among the 9 odd-numbered
175 years, fire activities in years 2003/2011/2013 show the highest three BC emission, which is also
176 consistent with results from the GFEDv4.1s dataset. Hence, the two independent fire emission
177 inventories agree on the interannual variation of fire activities.

178 Apart from cross-checking different fire emission inventories, we further validated the variability
179 of fire activities by investigating fire-induced changes in AOD (Fig. 1c). BC AOD from MERRA-
180 2 reanalysis and AOD of biomass burning aerosol type from CALIPSO were adopted to represent
181 fire activities. Basically, the interannual variation of fire-related AOD in both datasets agrees well
182 with the estimates from fire inventories, thus providing additional support for the quasi-biennial
183 variability of fire activities in the peak burning months over SMCA. Overall, the intercomparison
184 between multiple datasets indicates a consistent quasi-biennial variability in different fire

185 characteristics, including fire-consumed dry matter, fire-emitted aerosols as well as fire-related
186 changes in optical properties. Note that among the four datasets, the GFEDv4.1s inventory and
187 MERRA-2 reanalysis data provide data till the year of 2023, and the quasi-biennial variability in
188 the extended time series remains robust till 2023 (Fig. S1). To describe this quasi-biennial
189 variability for convenience, we hereafter refer to the odd-numbered (even-numbered) years that
190 have higher (lower) fire consumptions of dry matter than adjacent years as strong (weak) fire years.

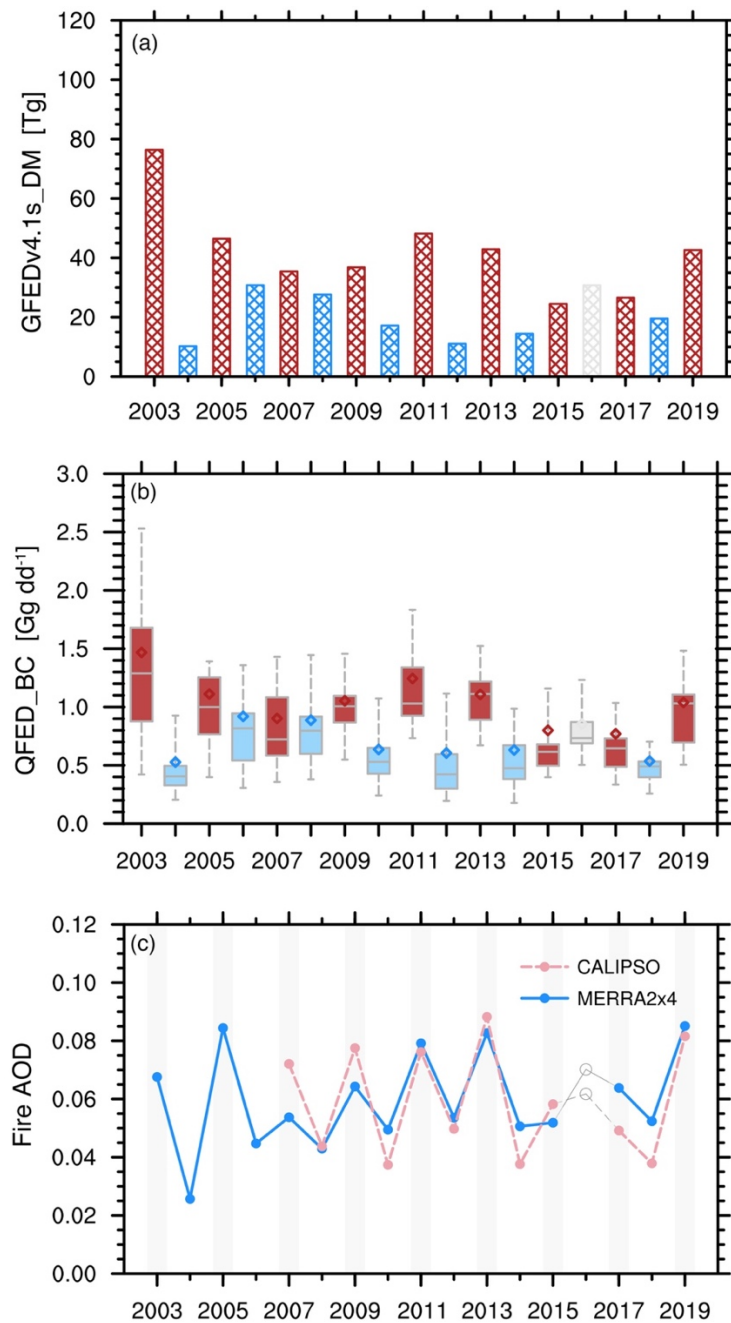


Figure 1. Interannual variations of different fire characteristics during the peak burning season (Apr-May) over Southern Mexico and Central America (SMCA). (a) Regional sum of the total dry matter consumed by fire activities based on the GFEDv4.1s emission data. (b) Distributions of the daily sum of fire-emitted black carbon (BC) over SMCA based on QFED emission data. Boxes denote the 25th and 75th percentiles. Bars outside the boxes denote the 10th and 90th percentiles. Bars within the boxes denote the medium values, and dots denote regional mean values (c) Regional mean aerosol optical depth (AOD) of smoke aerosols from CALIPSO product and BC AOD from MERRA-2 reanalysis. The odd-numbered years with strong fires are denoted by the grey bars.

204 **3.2 Dominant role of the biennial variability of precipitation**

205 Fire activity is strongly affected by factors including fire ignition, fuel load, and climate-weather
206 conditions (Flannigan et al., 2005; Archibald, 2016; Ichoku et al., 2016; Veira et al., 2016). Fire
207 ignition is affected by both natural lightning and human activities (Pechony and Shindell, 2009).

208 Since there ~~ishas~~ no policy to regulate fire activities with periodicity, it is unlikely that human
209 impact is the major driving force. Fuel availability may play a role in the interannual variation of
210 fires. ~~After having examined the GPP (surrogate for fuel load) prior to the burning season, we~~
211 ~~found little evidence regarding the role of fuel availability in contributing to the interannual~~
212 ~~variation of fires (Fig. S3). Lower values of GPP are found in some strong fire years compared to~~
213 ~~their adjacent years, e.g., the years 2003 and 2005. Correlations between regional GPP and fire-~~
214 ~~consumed dry matter are even slightly negative, but there is little evidence for it in the leaf area~~
215 ~~index, our surrogate for fuel load (Fig. S2). Correlations between LAI previous to the burning~~
216 ~~season and fire consumption are statistically insignificant.~~

217 Close yet complex relationships between ambient conditions (e.g., humidity, temperature,
218 precipitation) and fire activities have been widely revealed in previous studies (Cary et al., 2006;
219 Gillett et al., 2004; Prasad et al., 2008). For example, warm temperatures could increase fire
220 activity by increasing evapotranspiration and also by lengthening fire duration, while both the
221 timing and amount of precipitation could regulate fire behavior. To identify the climatic factors
222 that might be responsible for the quasi-biennial variation of fire activities, we first examined the
223 relationships between fire-~~consumed dry matter-consumption~~ and different meteorological
224 variables (Table 1). Temporal correlations of their regional mean values indicate that fire activities
225 are enhanced with warmer mean and maximum temperature ($R=0.47$ and 0.59), but are weakened
226 with higher precipitation ($R=-0.69$). Though wind speed could affect the spread of fire activities,
227 the insignificant correlation signifies a minor influence on the interannual scale (Fig. S3). ~~Other~~
228 ~~meteorological metrics such as vapor pressure deficit (VPD) and relative humidity (RH) are also~~
229 ~~frequently used to help understand fire-meteorology interactions. Here we found the interannual~~
230 ~~variations of regional mean VPD and RH are highly correlated with precipitation ($R = -0.8$ for VPD~~
231 ~~and $R=0.7$ for RH, respectively) and temperature ($R = 0.7$ for VPD and $R = -0.5$ for RH,~~
232 ~~respectively) over the SMCA region.~~

233 Figure 2 shows the spatial distribution of correlations of fire-~~consumed dry matter-consumption~~
234 with precipitation and mean temperature during peak burning months. With respect to

235 precipitation, negative correlations cover almost the entire SMCA region and are statistically
 236 significant over major fire source areas from Yucatan extending southwestward to Chiapas. In
 237 contrast, positive correlations between fire-consumed dry matter and maximum temperature
 238 mainly appear over the northern part of SMCA (southern Mexico), albeit with less influence over
 239 Central America (e.g., fire source areas in Guatemala). Hence, the interannual variability of
 240 precipitation affects the variation of fire activities on a wider spatial range. We next examined
 241 closely the time series of regional mean precipitation and temperature (Fig 3). Here regional mean
 242 values are calculated using data over land so that only climate conditions that could directly affect
 243 fire activities are considered. Two independent precipitation datasets show similar temporal
 244 evolution patterns. An obvious quasi-biennial variability is seen in regional mean precipitation.
 245 More suppressed precipitation (compared to adjacent years) corresponds well to the strong fire
 246 years (excluding the year 2016). Furthermore, spectral analysis confirms a statistically significant
 247 periodicity of approximately 2 years (0.042 cycles per month) for precipitation, suggesting the
 248 mediation of precipitation on the quasi-biennial feature of fire activities. Meanwhile, the quasi-
 249 biennial signal is less apparent in mean and maximum temperatures. For instance, temperatures in
 250 the strong fire years 2007 and 2009 are smaller in magnitude compared to adjacent weak fire years.
 251 Nevertheless, higher mean and maximum temperatures (compared to adjacent years) appear in
 252 2003 and 2011, which combines with the suppressed precipitation, contributing to the abnormally
 253 high fire-consumed dry matter consumption in the two years. As a result, while both temperature
 254 and precipitation are critical in shaping fire activities over the SMCA region, precipitation plays a
 255 more fundamental role in formulating the quasi-biennial variability of fires.

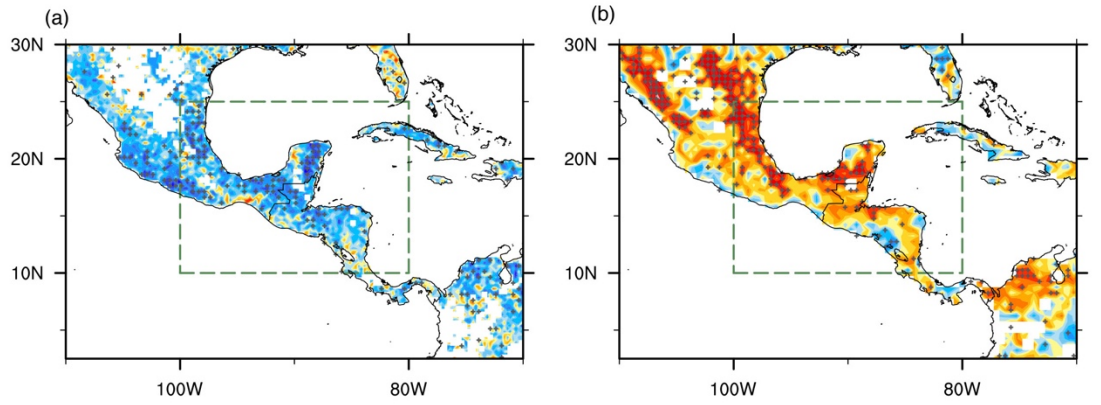
256

257 **Table 1.** Correlations between the regional sum of fire consumed dry matter based on the
 258 GFEDv4.1 data and regional mean values of different meteorological variables (including the
 259 monthly mean precipitation from IMERG dataset, mean temperature, maximum temperature from
 260 CRU dataset, and 10m wind speed from ERA5 reanalysis) averaged in the peak fire season (April-
 261 May).

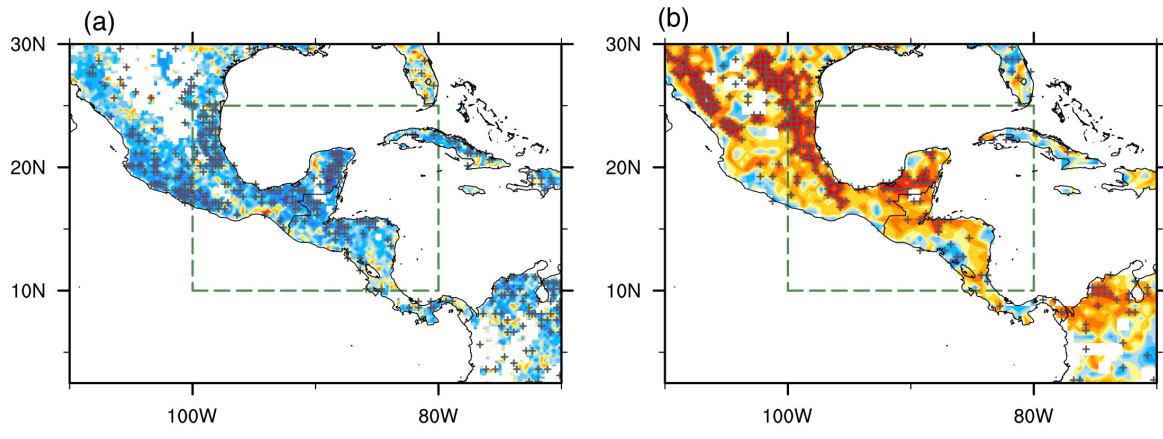
Correlation	Precipitation	Mean Temperature	Maximum Temperature	10m wind speed
Fire-consumed Dry matter	-0.69*	0.47*	0.59*	0.29

262 * represents the correlations are statistically significant at the 90% confidence level based on the
 263 student's T-test.

264

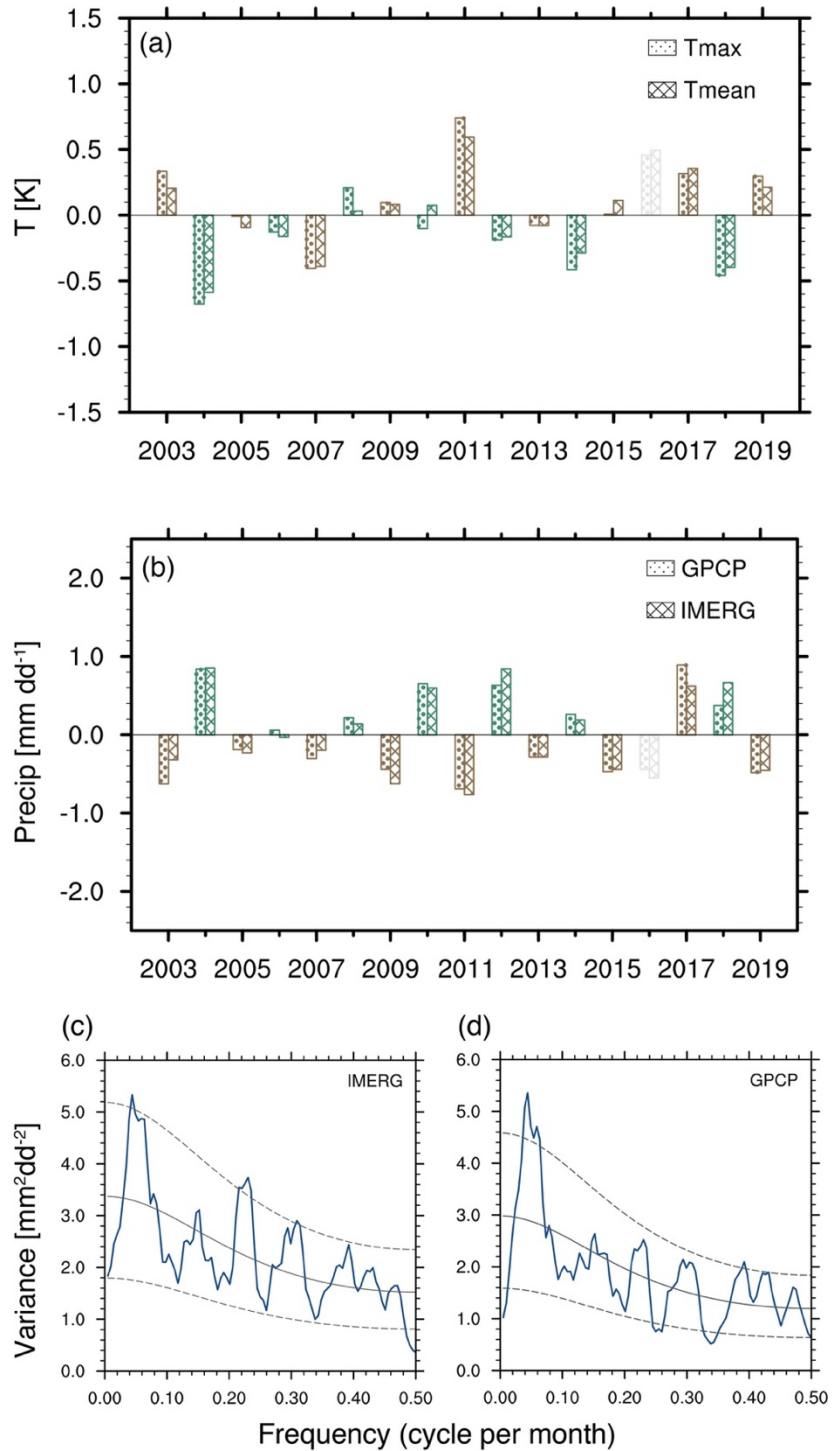


265
266



267
268
269
270
271
272
273

Figure 2. The influence of meteorological factors on fire activities over SMCA. Spatial distributions of grid-to-grid correlations between fire-consumed dry matter and (a) precipitation from IMERG and (b) maximum temperature from CRU during the peak fire season (Apr-May) over 2003-2019. Stippling indicates the correlations are statistically significant at the 90% confidence level based on the student's T-test. The green boxes denote the SMCA region.

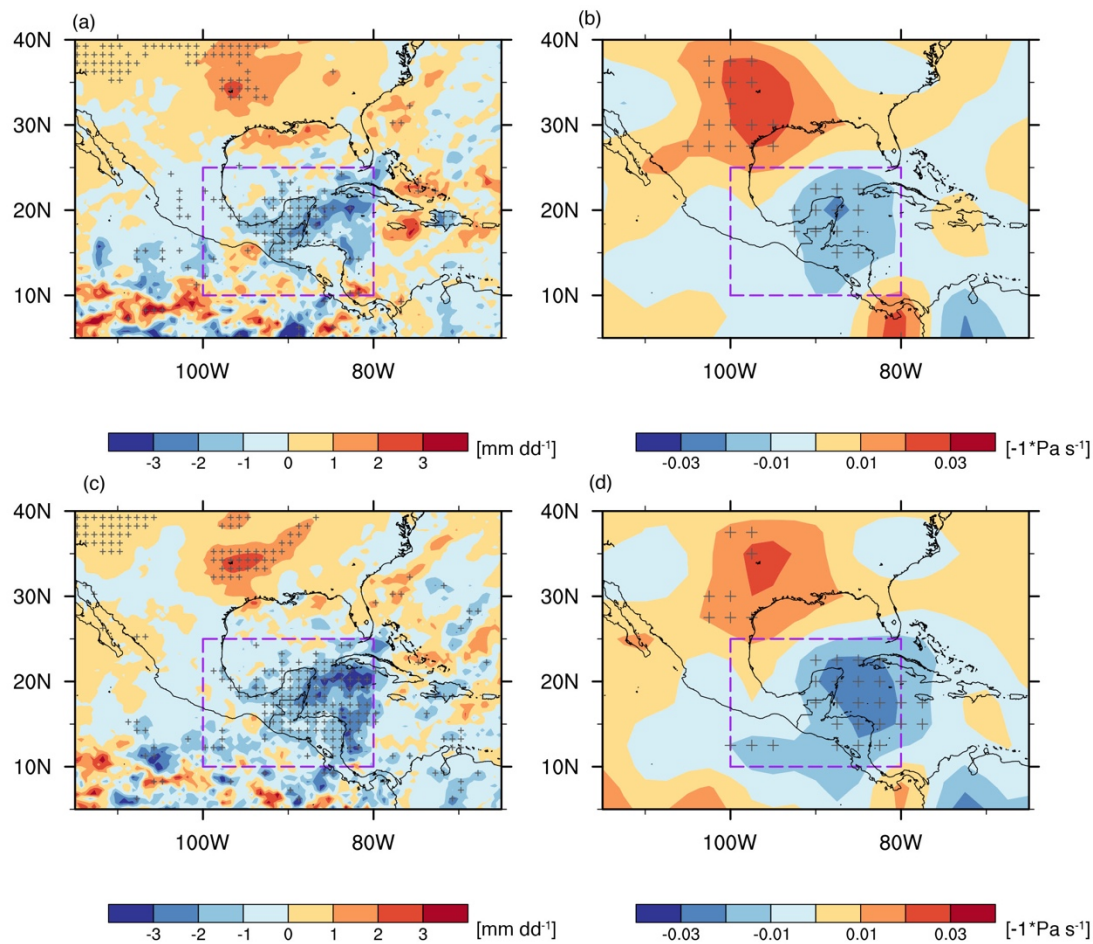


274
 275 **Figure 3.** Interannual variability of meteorological factors in peak fire season over SMCA. Time
 276 series of the Apr-May (a) mean/maximum temperature and (b) mean precipitation anomalies [\(with
 277 respect to the 2003-2019 climatology mean\)](#) averaged over SMCA (land only). (c) Spectral
 278 analysis of monthly mean precipitation averaged over SMCA during 2003-2019. The black solid
 279 line and dashed lines represent the red noise curve and the 10%, 90% confidence interval.
 280
 281

282 The leading role of precipitation on the interannually varying fire activities is evident in the
283 composite analysis, as shown by the contrast of reduced precipitation in strong fire years and
284 enhanced precipitation in weak fire years (Fig. 4a). The composite analysis further shows that the
285 anomalous precipitation is closely related to vertical motions, with stronger subsidence
286 corresponding to weaker precipitation (Fig. 4b). It is worth noting that to the northwest of the
287 SMCA region near the southeast US, composited precipitation and vertical velocity also differ
288 significantly between strong and weak fire years albeit of opposite signs. Consistent changing
289 features of precipitation and vertical velocity are also captured when regressing the two variables
290 on the regional mean precipitation over SMCA (Fig. 4c-d). The negative regression coefficients
291 indicate a stronger upward (downward) motion corresponding to higher (weaker) precipitation. In
292 sum, for a specific year, stronger subsidence and the subsequent suppression of precipitation tend
293 to amplify fire activity in that year, and vice versa for the year with weakened subsidence and less
294 suppression effect of precipitation. In this way, the quasi-biennial variability of precipitation leads
295 to the same interannual variability of fire activities.

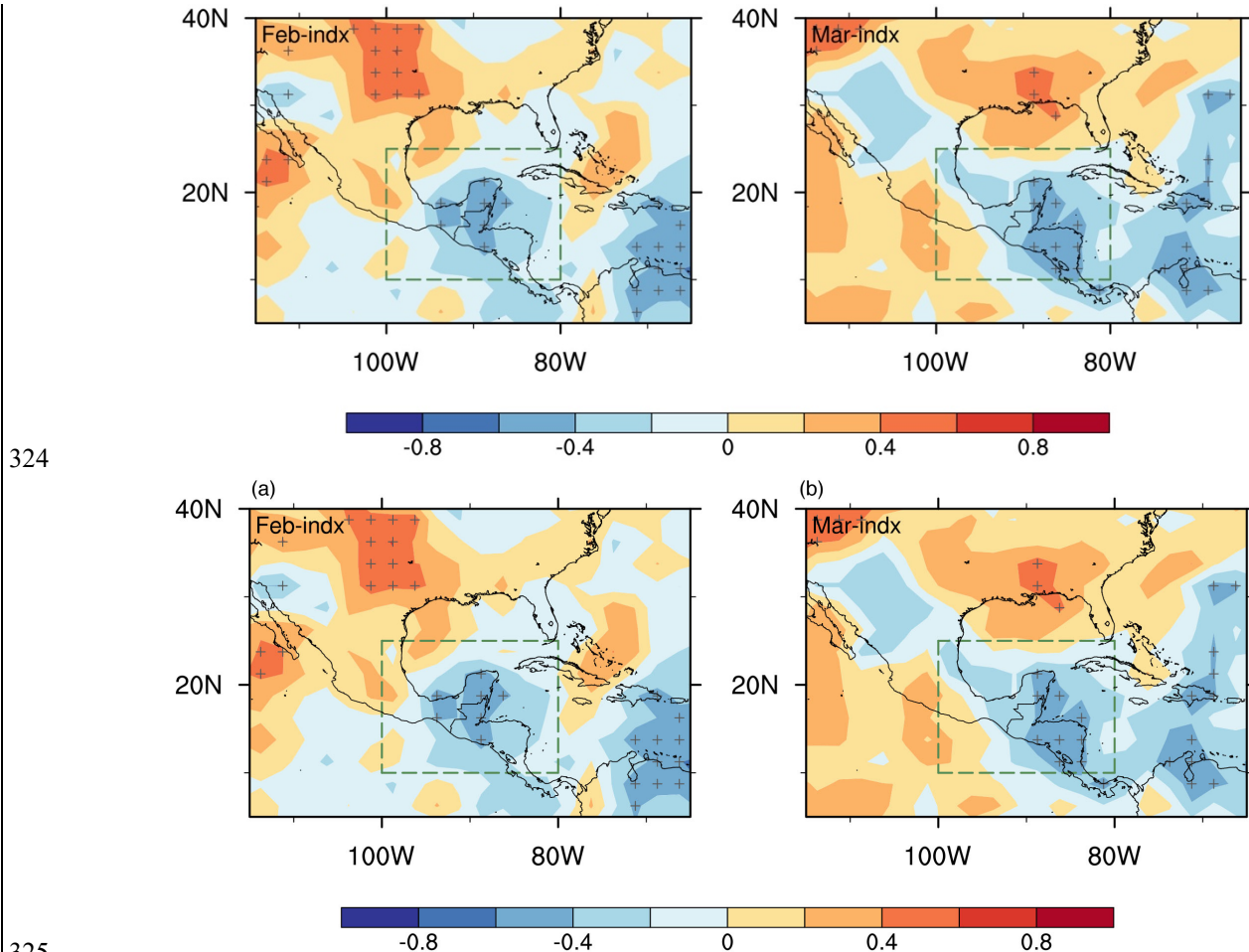
296 Precipitation patterns over the SMCA region and the variability are associated with complex
297 physical forcing mechanisms, e.g. changes in sea surface temperature, low-level winds, the
298 strength and position of ITCZ et al., and all of these processes could be modulated by large-scale
299 modes of atmospheric and oceanic variability (Duran-Quesada et al., 2017; Perdigon-Morales et
300 al., 2019; Amador et al., 2006). Here we chose 10 typical teleconnection patterns, for example, the
301 El Niño-Southern Oscillation, (ENSO), based on previous studies and examined their relationships
302 with SMCA precipitation in the peak fire months. After calculating the correlations between Apr-
303 May mean precipitation and the index in varying months (both simultaneously and previous to the
304 fire season), we found that the precipitation in the fire season is mostly affected by the East
305 Pacific/North Pacific Oscillation (EP/NP) pattern in the previous two months (Feb-Mar).
306 Generally, the positive phase of EP/NP features negative height anomalies and an enhanced
307 cyclonic circulation over the eastern United States (Athanasiadis et al., 2010). Consequently, in
308 the following fire season, this causes anomalous upward and downward motions over the
309 southeastern US and the SMCA region respectively (Fig. S43), and enhances precipitation over
310 the southeastern US yet suppressing precipitation over the SMCA region (Fig. 5). Hence, the
311 EP/NP teleconnection results in an opposite responding pattern in precipitation and vertical

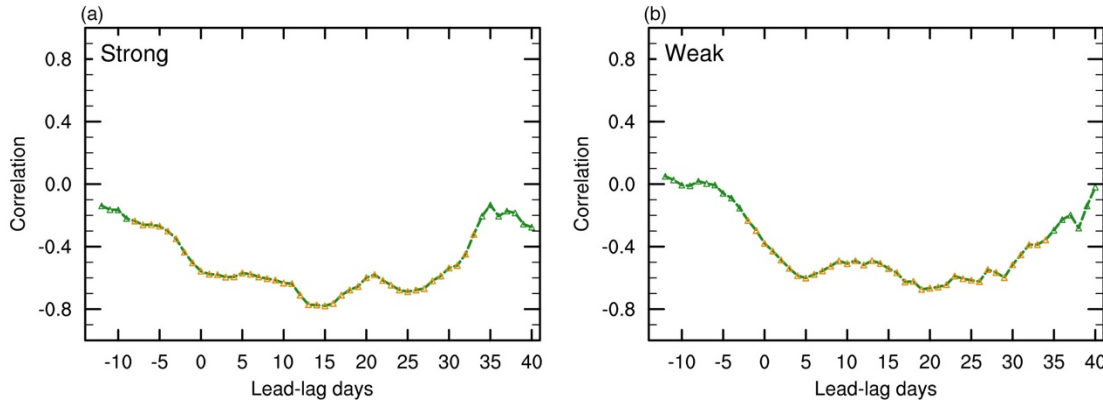
312 velocity between the eastern US and the SMCA region. This further explains the similar
313 contrasting spatial pattern that is found in the aforementioned composite and regression analysis.



316 **Figure 4.** Varying characteristics of precipitation and circulations. Differences of composites of
317 (a) precipitation and (b) 500hPa vertical pressure velocity (reversed signs) between strong and
318 weak fire years. Stippling indicates the differences are statistically significant at the 90%
319 confidence level based on T-test. Regressions of Apr-May mean (c) precipitation and (d) 500hPa
320 vertical velocity on the regional mean precipitation over SMCA (reversed signs) during 2003-
321 2019. Stippling indicates regression coefficients are statistically significant at the 90% confidence
322 level based on the T-test.

323





334

335 **Figure 6.** Different duration of fire-precipitation interaction. Lead-lag correlations between
 336 regional mean daily precipitation and fire emission composites in (a) strong fire years and (b) weak
 337 fire years over SMCA. Positive lead-lag days represent that precipitation leads while negative lead-
 338 lag days represent fire emissions leads. Correlations that are statistically significant at the 90%
 339 confidence level based on Student's t-test are marked with yellow triangles.

340

341 **3.3 Positive feedback between enhanced fire emissions and suppressed precipitation**

342 Previous studies have found that fire-emitted aerosols could interact with synoptic weather, which
343 in turn affects fire variability (Huang et al., 2023). In view of this, one concern is if fire and
344 precipitation interact on short timescales (i.e., within individual fire seasons) in our case over the
345 SMCA region, and if so, how this feedback modulates the quasi-biennial variability of
346 precipitation and fire activities. We first calculated lead-lag correlations between daily
347 precipitation and fire emissions to identify the short-term fire-precipitation interaction. As shown
348 in Fig. 6 lead-lag correlations between regional mean precipitation and fire emission are generally
349 similar whether fire activities in strong or weak fire years are considered. When precipitation leads,
350 precipitation negatively correlates with fire emission for more than 20 days, signifying a long-
351 lasting suppression effect of precipitation on fire activities. In other words, weakened precipitation
352 would enhance fire activities. Meanwhile, when fire leads, negative correlations indicate that
353 increased fire activities would further suppress precipitation at shorter timescales (3-5 days)
354 through rapid adjustments. In short, there is a two-way interaction between precipitation and fire
355 activities on short timescales with different duration, forming a positive feedback loop.

356 We also conducted sensitivity simulations to investigate the underlying processes involved in the
357 fire-precipitation feedback. Fig. 7 shows the simulated difference in AOD (referred to as fire AOD)
358 between Case_Strong and Case_Weak. Both the spatial pattern and magnitude agree well with the
359 difference in AOD between strong and weak fire years based on CALIPSO observations.
360 Compared to the spatial patterns of fire consumption in Fig. 7, we can clearly see two transport
361 pathways of fire-emitted aerosols due to the continental divide by the Central Mexican Plateau.
362 North of 15°N, fire-emitted aerosols are transported northward by the subtropical high, among
363 which large amounts accumulate over the downstream Gulf of Mexico due to the block of the high
364 terrain, and the rest is further transported northward reaching the southeastern US; South of 15°N,
365 prevailing easterlies transport fire-emitted aerosols directly westward, far away to the eastern
366 Pacific.

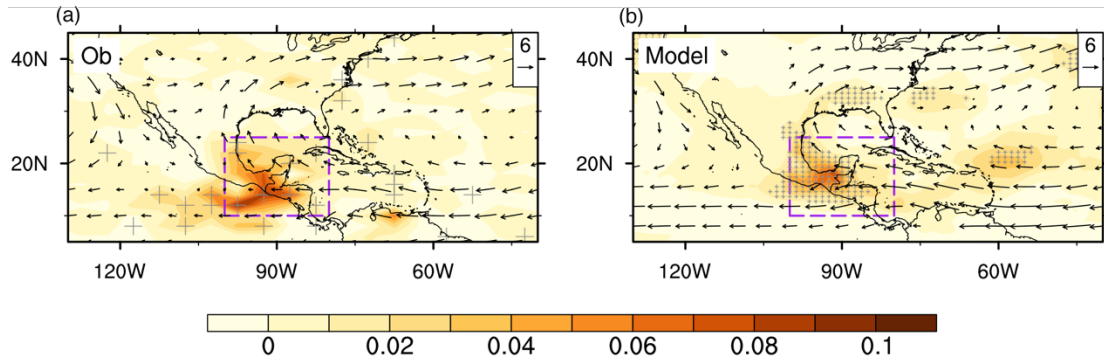


Figure 7. Evaluation of model simulated fire-induced AOD. (a) Spatial distributions of differences in biomass burning AOD between strong and weak fire years from CALIPSO satellite data. (b) Differences in simulated AOD between Case_Strong and Case_Weak. Mean 850hPa wind vectors from (a) NCEP reanalysis data averaged in all years and (b) model simulations averaged between both cases are overlaid respectively. Stippling indicates the differences in AOD are statistically significant based on T-test.

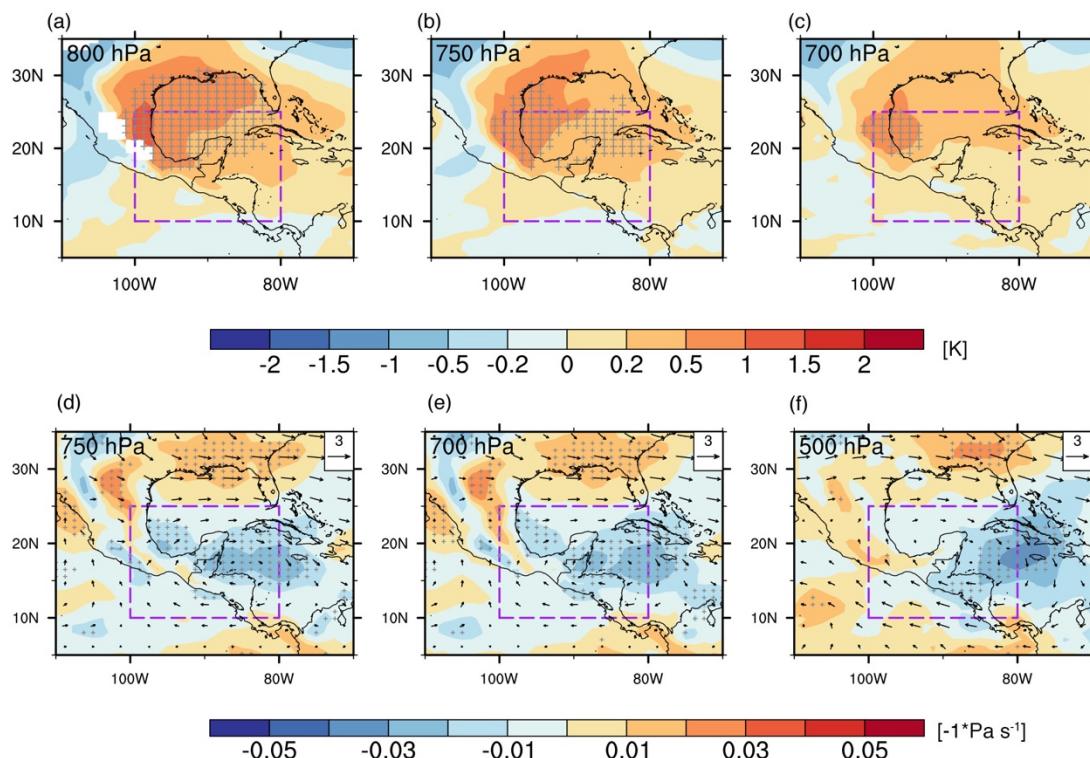


Figure 8. Changes in meteorological variables induced by fire-emitted aerosols. Differences in (a-c) atmospheric temperature and (d-f) vertical pressure velocity (reversed signs and shaded colors) at different vertical levels between Case_Strong and Case_Weak. Changes in horizontal winds between the two cases are overlaid in (d-f). Stippling indicates the differences are statistically significant at the 90% confidence level based on T-test.

383 Considering the northward pathway, with the stack of light-absorbing BC aerosols, air temperature
384 warms up by approximately 1-2K, and this warming extends from 800hPa to 700hPa where BC
385 aerosols suspend (Fig. 8a-c). Vertical slices of the temperature anomalies indicate significant
386 warming to the north (downstream) of the fire source regions (Fig. 9a). In response to this warming,
387 the air above the fire aerosol layers rises up (Fig. 8d-f). The anomalous ascending motion covers
388 from the Gulf of Mexico to the southeastern US, with the maximum center located near the Gulf
389 of Mexico. This abnormal ascending motion, on one hand, enhances precipitation downstream of
390 the fire source regions, and on the other hand forces a compensating anomalous descending motion
391 over the SMCA region and suppresses the precipitation over the fire source regions (Fig. 9b-c).
392 This simulated opposite change in precipitation resembles the spatial pattern of the composited
393 precipitation difference between strong and weak fire years (Fig. 4a), suggesting that fire-
394 precipitation interaction reinforces the contrast of precipitation between strong and weak fire years.
395 Therefore, the model simulations confirm a positive fire-precipitation feedback loop on the short
396 timescale within the fire season.

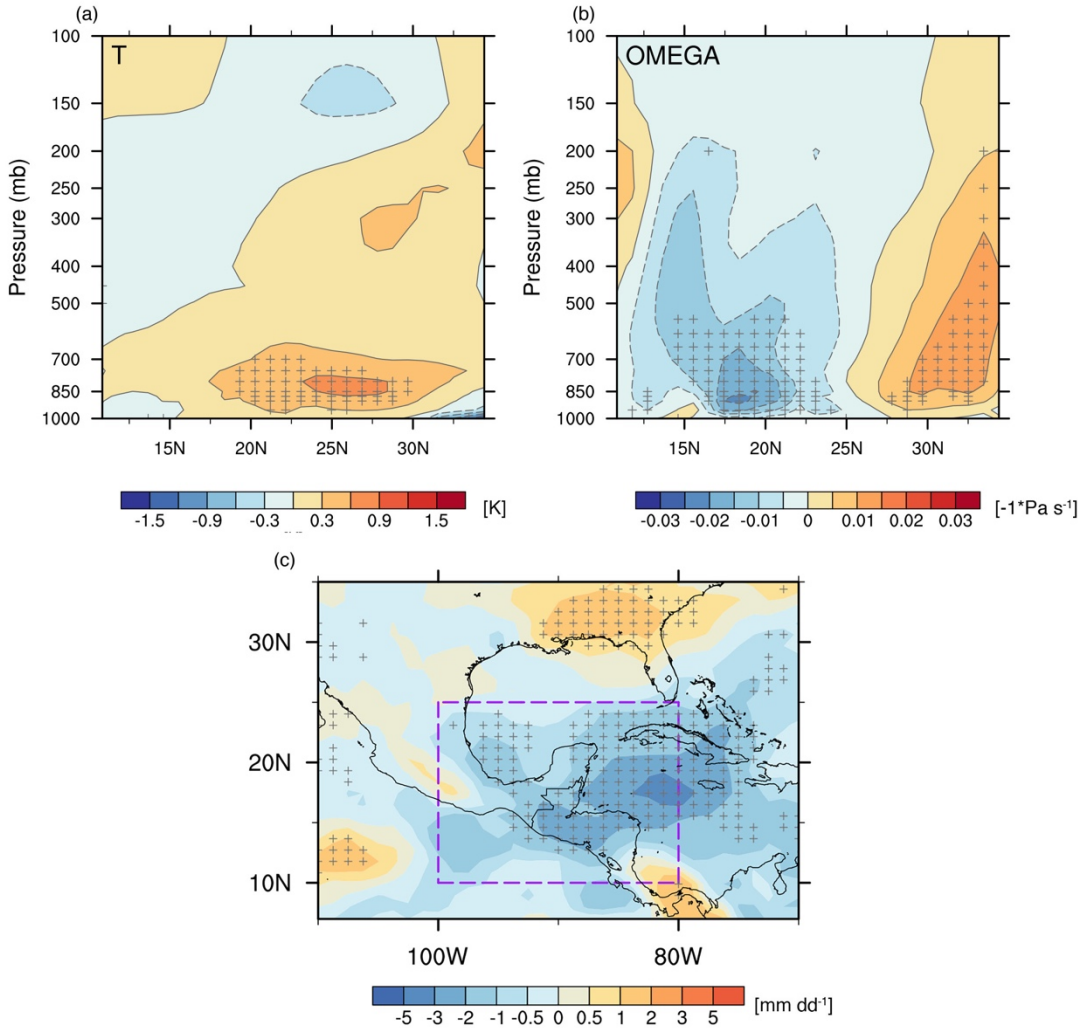


Figure 9. Vertical slices of differences in (a) atmospheric temperature and (b) pressure velocity averaged along $[80^{\circ} - 100^{\circ} \text{W}]$ between Case_Strong and Case_Weak. (c) Differences in precipitation between Case_Strong and Case_Weak. Stippling indicates the differences are statistically significant based on T-test.

As illustrated in Fig. 10, originally on the interannual scale, fire activities over the SMCA region exhibit a significant quasi-biennial variability that is predominantly determined by the quasi-biennial variation of precipitation. On this basis, there is an additional two-way interaction between fire and precipitation on short timescales. Typically, precipitation suppresses fire activities with a time lag of more than 20 days, while fire-emitted aerosols suppress precipitation by modifying circulations with a timescale of 3-5 days. That is to say, for a year with abnormally weak precipitation, fire activities would get amplified, which in turn further weakens precipitation. In

397

398

399

400

401

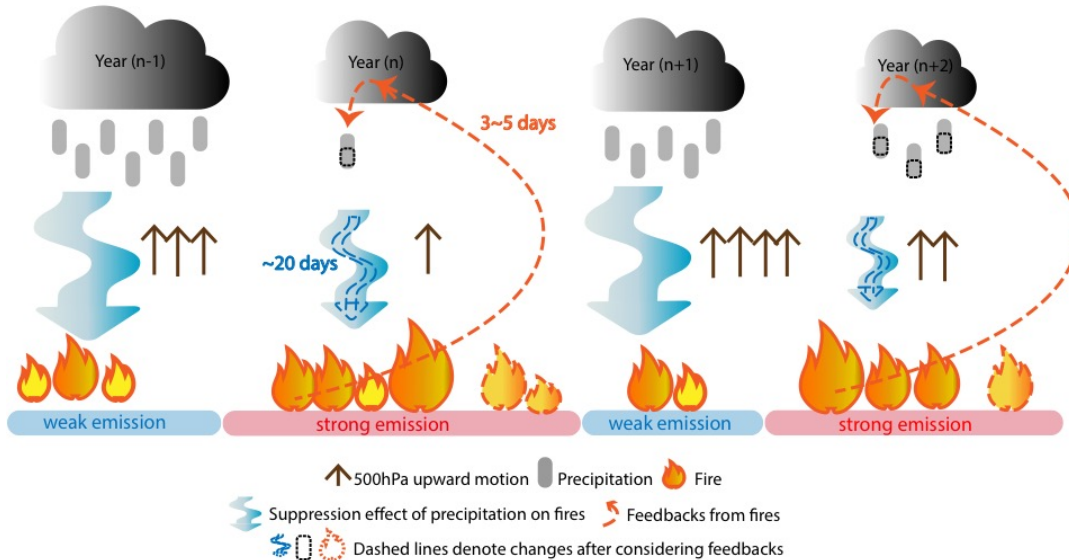
402

403

411 this way, the short-term positive feedback loop ultimately enhances the quasi-biennial variability
412 of precipitation and fire activities over the SMCA region.

413

414



415
416 **Figure 10.** A schematic diagram illustrating how multi-scale fire-precipitation interactions shape
417 the quasi-biennial variability of fires over SMCA. On the interannual scale, the quasi-biennially
418 varying precipitation triggers a similar quasi-biennial variability of fire activities via its
419 suppression effect. Compared to adjacent years, a weaker precipitation year will facilitate stronger
420 fires. On short timescales within each fire season, there is a positive feedback loop between fire
421 and precipitation (denoted by dashed lines). The suppression effect of precipitation lasts long for
422 approximately 20 days, while fires affect precipitation through a rapid adjustment of 3-5 days. In
423 the weaker precipitation year, stronger fire activities emit more aerosols, which by mediating
424 temperature and circulations, ultimately suppress precipitation over the fire source region. Such
425 short-term interactions between precipitation and fire amplify the magnitude of anomalous fire and
426 precipitation in individual years and enhance the quasi-biennial variability of both precipitation
427 and fire.

428 **4 Conclusion and Discussion**

429 Fires play an important role in the Earth system, and the complex interaction between fire activities
430 and ambient conditions poses a great challenge to fire prediction and management. This study
431 identifies a distinct quasi-biennial variability of fire activities over the SMCA region during 2003-
432 2019 on the basis of different fire metrics. Both the bottom-up (GFEDv4.1s) and top-down(QFED)
433 emission inventories show relatively higher fire consumption (or emission) in the odd-numbered
434 years than the adjacent even-numbered years with the only exception of the year 2016. Moreover,
435 fire-induced changes in AOD also reveal consistent quasi-biennial variation.

436 By examining the relationships between fire consumption and different meteorological variables,
437 our analysis indicates that the quasi-biennial signal is dominated by the quasi-biennially varying
438 precipitation, while the influence of temperature is mostly reflected in a few extremely strong fire
439 years. Typically, strong fire years correspond to suppressed upward motions and weakened
440 precipitation. The quasi-biennial variability of precipitation is seen in the time series of the regional
441 mean precipitation over SMCA and the spectral analysis, and is closely related to the EP-NP
442 teleconnection pattern in the two months previous to the fire season. The positive phase of the EP-
443 NP pattern implies enhanced precipitation over the southeastern US (downstream of the SMCA),
444 albeit reduced precipitation over the SMCA region.

445 On the other hand, we further found that positive feedback exists between fire-emitted aerosols
446 and precipitation on short timescales and acts to amplify the quasi-biennial oscillations in both fire
447 and precipitation over the SMCA region. Lead-lag correlations between daily fire emission and
448 precipitation suggest that the two-way interactions occur with different duration. The suppression
449 effect of precipitation lasts for approximately 20 days, while fire-emitted aerosols weaken
450 precipitation through rapid adjustments of 3-5 days. Furthermore, model simulations reveal that
451 compared to weak fire years, more fire-emitted aerosols are transported downstream and
452 accumulate near the Gulf of Mexico in strong fire years. These suspended light-absorbing BC
453 aerosols warm the low-level atmosphere by 1-2K and induce anomalous ascending motion aloft
454 700hPa. A compensating descending motion is subsequently forced over the SMCA region, which
455 ultimately suppresses the precipitation over the fire source region and hence forms a positive
456 feedback loop.

457 These findings provide useful information relevant to the fire control and mitigation of air quality
458 over the SMCA region. Given that fire activities over the SMCA represent a typical tropical fire
459 regime, our work may also provide new insight into some fundamental features of fires in the Earth
460 System. The mechanism may also operate elsewhere useful on the planet. While precipitation is
461 demonstrated to play the primary role in determining the periodicity of fire activities over the
462 SMCA region, the fundamental cause of the quasi-biennial variability of precipitation is unknown.
463 Currently, we have only shown that the EP-NP teleconnection, among all selected indexes, exerts
464 the most influence on the interannual variability of precipitation. Other teleconnection patterns,
465 e.g., ENSO, despite their insignificant correlations with SMCA precipitation, may affect the
466 circulation and precipitation over the southeastern US or over the neighboring Intra-American Sea
467 (Anthony Chen and Taylor, 2002), and hence might more or less affect the precipitation over the
468 SMCA region. Moreover, though we demonstrated positive feedback between fire-emitted
469 aerosols and precipitation exists on short timescales, to what extent this feedback contributes to
470 the quasi-biennial variability of fire activities remains unquantified due to the absence of coupled
471 fire-climate interactions in current model simulations. Future efforts to quantify how different
472 factors and feedback work together and to shape the quasi-biennial variability of precipitation and
473 fire activities using interactive fire-climate models would further benefit the prediction and
474 management of fire activities over the SMCA region.

475 **Data availability**

476 The GFED v4.1s fire emission data is available at <http://www.globalfiredata.org/data.html>.
477 The CRU TS v.4.06 can be found at <https://crudata.uea.ac.uk/cru/data/hrg/>. The QFEDv2.5 data
478 can be found at <http://ftp.as.harvard.edu/gcgrid/data/ExtData/HEMCO/QFED/v2018-07/>.
479 ~~The AVHRR leaf area index is available from <https://www.ncei.noaa.gov/access/metadata/landing-page/bin/iso?id=gov.noaa.nedc:C01559>. The MODIS GPP data is available from <https://lpdaac.usgs.gov/products/mod17a2hv061/>~~
480 -The MERRA-2 reanalysis data can be found at https://gmao.gsfc.nasa.gov/reanalysis/MERRA-2/data_access/. The IMERG precipitation dataset
481 can be obtained from <https://gpm.nasa.gov/data/imerg>. The GPCP dataset can be obtained from
482 <https://www.ncei.noaa.gov/products/climate-data-records/precipitation-gpcp-daily>.
483 Teleconnection indices can be found at <https://psl.noaa.gov/data/climateindices/list/>. The NCEP-
484 NCAR reanalysis is obtained from
485 <https://www.esrl.noaa.gov/psd/data/gridded/data.ncep.reanalysis2.html>.
486 The CALIPSO product is available at
487 https://asdc.larc.nasa.gov/project/CALIPSO/CAL_LID_L3_Tropospheric_APro_AllSky-Standard-V4-20_V4-20.
488

491
492 **Author contribution**

493 Y.L. and Y. Q. conceived of the presented idea. Y. Q., Y. W. and Y. L. developed the theory. Y.
494 L. performed the computations and verified the methods. Y. Q., Y. L. and K. Z wrote the first draft
495 of the manuscript. All authors contributed to the interpretation of the results and writing/revision
496 of the final manuscript.

497
498 **Competing interests**

499 Yun Qian and Hailong Wang are members of the editorial board of Atmospheric Chemistry and
500 Physics. The authors have no other competing interests to declare.

501
502 **Acknowledgments**

503 We benefited from discussing some aspects of this work with John M Wallace and Dae-Hyun Kim.
504 ~~Yawen Liu is supported by the National Natural Science Foundation of China (No. 42325506).~~
505 This study is ~~also~~ supported by the U.S. Department of Energy's Office of Science as part of the
506 Regional and Global Modeling and Analysis program. The Pacific Northwest National Laboratory
507 is operated for DOE by Battelle Memorial Institute under contract DE-AC05-76RL01830. We are
508 grateful to the High-Performance Computing (HPC) and the Massive Data Center (MDC) at
509 Nanjing University for ~~doing~~the numerical calculations.

514 **References**

515 Abram, N. J., Henley, B. J., Sen Gupta, A., Lippmann, T. J. R., Clarke, H., Dowdy, A. J., Sharples, J. J.,
516 Nolan, R. H., Zhang, T. R., Wooster, M. J., Wurtzel, J. B., Meissner, K. J., Pitman, A. J., Ukkola, A. M.,
517 Murphy, B. P., Tapper, N. J., and Boer, M. M.: Connections of climate change and variability to large and
518 extreme forest fires in southeast Australia, *Commun Earth Environ*, 2, ARTN 810.1038/s43247-020-00065-
519 8, 2021.

520 Adler, R. F., Sapiano, M. R. P., Huffman, G. J., Wang, J. J., Gu, G. J., Bolvin, D., Chiu, L., Schneider, U.,
521 Becker, A., Nelkin, E., Xie, P. P., Ferraro, R., and Shin, D. B.: The Global Precipitation Climatology Project
522 (GPCP) Monthly Analysis (New Version 2.3) and a Review of 2017 Global Precipitation, *Atmosphere*, 9,
523 ARTN 1310.3390/atmos9040138, 2018.

524 Adler, R. W., Jian-Jian; Sapiano, Mathew; Huffman, George; Bolvin, David; Nelkin, Eric; and NOAA CDR
525 Program: Global Precipitation Climatology Project (GPCP) Climate Data Record (CDR), Version 1.3
526 (Daily), NOAA National Centers for Environmental Information. doi:10.7289/V5RX998Z, 2017.

527 Aguilera, R., Corringham, T., Gershunov, A., and Benmarhnia, T.: Wildfire smoke impacts respiratory
528 health more than fine particles from other sources: observational evidence from Southern California, *Nature*
529 *Communications*, 12, ARTN 149310.1038/s41467-021-21708-0, 2021.

530 Amador, J. A., Alfaro, E. J., Lizano, O. G., and Magana, V. O.: Atmospheric forcing of the eastern tropical
531 Pacific: A review, *Prog Oceanogr*, 69, 101-142, 10.1016/j.pocean.2006.03.007, 2006.

532 Anthony Chen, A. and Taylor, M. A.: Investigating the link between early season Caribbean rainfall and
533 the El Niño + 1 year, *International Journal of Climatology*, 22, 87-106, 10.1002/joc.711, 2002.

534 Archibald, S.: Managing the human component of fire regimes: lessons from Africa, *Philosophical
535 Transactions of the Royal Society B: Biological Sciences*, 371, 20150346, 2016.

536 Athanasiadis, P. J., Wallace, J. M., and Wettstein, J. J.: Patterns of Wintertime Jet Stream Variability and
537 Their Relation to the Storm Tracks, *J Atmos Sci*, 67, 1361-1381, 10.1175/2009jas3270.1, 2010.

538 Bond, T. C., Doherty, S. J., Fahey, D., Forster, P., Berntsen, T., DeAngelo, B., Flanner, M., Ghan, S.,
539 Kärcher, B., and Koch, D.: Bounding the role of black carbon in the climate system: A scientific assessment,
540 *Journal of Geophysical Research: Atmospheres*, 118, 5380-5552, 2013.

541 Bowman, D. M., Balch, J. K., Artaxo, P., Bond, W. J., Carlson, J. M., Cochrane, M. A., D'Antonio, C. M.,
542 DeFries, R. S., Doyle, J. C., and Harrison, S. P.: Fire in the Earth system, *science*, 324, 481-484, 2009.

543 Bowman, D. M. J. S., Williamson, G. J., Abatzoglou, J. T., Kolden, C. A., Cochrane, M. A., and Smith, A.
544 M. S.: Human exposure and sensitivity to globally extreme wildfire events, *Nat Ecol Evol*, 1, ARTN
545 005810.1038/s41559-016-0058, 2017.

546 Cary, G. J., Keane, R. E., Gardner, R. H., Lavorel, S., Flannigan, M. D., Davies, I. D., Li, C., Lenihan, J.
547 M., Rupp, T. S., and Mouillot, F.: Comparison of the sensitivity of landscape-fire-succession models to
548 variation in terrain, fuel pattern, climate and weather, *Landscape ecology*, 21, 121-137, 2006.

549 Crounse, J., DeCarlo, P., Blake, D. R., Emmons, L., Campos, T., Apel, E., Clarke, A., Weinheimer, A.,
550 McCabe, D., and Yokelson, R. J.: Biomass burning and urban air pollution over the Central Mexican
551 Plateau, *Atmospheric Chemistry and Physics*, 9, 4929-4944, 2009.

552 Crutzen, P. J. and Andreae, M. O.: Biomass Burning in the Tropics - Impact on Atmospheric Chemistry
553 and Biogeochemical Cycles, *Science*, 250, 1669-1678, DOI 10.1126/science.250.4988.1669, 1990.

554 Danabasoglu, G., Lamarque, J. F., Bacmeister, J., Bailey, D. A., DuVivier, A. K., Edwards, J., Emmons, L.
555 K., Fasullo, J., Garcia, R., Gettelman, A., Hannay, C., Holland, M. M., Large, W. G., Lauritzen, P. H.,
556 Lawrence, D. M., Lenaerts, J. T. M., Lindsay, K., Lipscomb, W. H., Mills, M. J., Neale, R., Oleson, K. W.,
557 Otto-Btiesner, B., Phillips, A. S., Sacks, W., Tilmes, S., van Kampenhout, L., Vertenstein, M., Bertini, A.,

558 Dennis, J., Deser, C., Fischer, C., Fox-Kemper, B., Kay, J. E., Kinnison, D., Kushner, P. J., Larson, V. E.,
559 Long, M. C., Mickelson, S., Moore, J. K., Nienhouse, E., Polvani, L., Rasch, P. J., and Strand, W. G.: The
560 Community Earth System Model Version 2 (CESM2), *J Adv Model Earth Sy*, 12, ARTN
561 e2019MS00191610.1029/2019MS001916, 2020.

562 Ding, K., Huang, X., Ding, A. J., Wang, M. H., Su, H., Kerminen, V. M., Petaja, T., Tan, Z. M., Wang, Z.
563 L., Zhou, D. R., Sun, J. N., Liao, H., Wang, H. J., Carslaw, K., Wood, R., Zuidema, P., Rosenfeld, D.,
564 Kulmala, M., Fu, C. B., Poschl, U., Cheng, Y. F., and Andreae, M. O.: Aerosol-boundary-layer-monsoon
565 interactions amplify semi-direct effect of biomass smoke on low cloud formation in Southeast Asia, *Nature
566 Communications*, 12, ARTN 641610.1038/s41467-021-26728-4, 2021.

567 Duran-Quesada, A. M., Gimeno, L., and Amador, J.: Role of moisture transport for Central American
568 precipitation, *Earth Syst Dynam*, 8, 147-161, 10.5194/esd-8-147-2017, 2017.

569 Fang, K. Y., Yao, Q. C., Guo, Z. T., Zheng, B., Du, J. H., Qi, F. Z., Yan, P., Li, J., Ou, T. H., Liu, J., He,
570 M. S., and Trouet, V.: ENSO modulates wildfire activity in China, *Nature Communications*, 12, ARTN
571 176410.1038/s41467-021-21988-6, 2021.

572 Fasullo, J. T., Rosenbloom, N., and Buchholz, R.: A multiyear tropical Pacific cooling response to recent
573 Australian wildfires in CESM2, *Science Advances*, 9, eadg1213, 2023.

574 Flannigan, M. D., Krawchuk, M. A., de Groot, W. J., Wotton, B. M., and Gowman, L. M.: Implications of
575 changing climate for global wildland fire, *International journal of wildland fire*, 18, 483-507, 2009.

576 Flannigan, M. D., Logan, K. A., Amiro, B. D., Skinner, W. R., and Stocks, B.: Future area burned in Canada,
577 *Climatic change*, 72, 1-16, 2005.

578 Gelaro, R., McCarty, W., Suarez, M. J., Todling, R., Molod, A., Takacs, L., Randles, C. A., Darmenov, A.,
579 Bosisovich, M. G., Reichle, R., Wargan, K., Coy, L., Cullather, R., Draper, C., Akella, S., Buchard, V.,
580 Conaty, A., da Silva, A. M., Gu, W., Kim, G. K., Koster, R., Lucchesi, R., Merkova, D., Nielsen, J. E.,
581 Partyka, G., Pawson, S., Putman, W., Rienecker, M., Schubert, S. D., Sienkiewicz, M., and Zhao, B.: The
582 Modern-Era Retrospective Analysis for Research and Applications, Version 2 (MERRA-2), *J Climate*, 30,
583 5419-5454, 10.1175/Jcli-D-16-0758.1, 2017.

584 Giglio, L., Randerson, J. T., and Werf, G. R.: Analysis of daily, monthly, and annual burned area using the
585 fourth - generation global fire emissions database (GFED4), *Journal of Geophysical Research: Biogeosciences*, 118, 317-328, 2013.

587 Gillett, N., Weaver, A., Zwiers, F., and Flannigan, M.: Detecting the effect of climate change on Canadian
588 forest fires, *Geophysical Research Letters*, 31, 2004.

589 Harris, I., Jones, P., Osborn, T., and Lister, D.: Updated high - resolution grids of monthly climatic
590 observations – the CRU TS3. 10 Dataset, *International Journal of Climatology*, 34, 623-642, 2014.

591 Hersbach, H., Bell, B., Berrisford, P., Hirahara, S., Horanyi, A., Munoz-Sabater, J., Nicolas, J., Peubey, C.,
592 Radu, R., Schepers, D., Simmons, A., Soci, C., Abdalla, S., Abellán, X., Balsamo, G., Bechtold, P., Biavati,
593 G., Bidlot, J., Bonavita, M., De Chiara, G., Dahlgren, P., Dee, D., Diamantakis, M., Dragani, R., Flemming,
594 J., Forbes, R., Fuentes, M., Geer, A., Haimberger, L., Healy, S., Hogan, R. J., Holm, E., Janiskova, M.,
595 Keeley, S., Laloyaux, P., Lopez, P., Lupu, C., Radnoti, G., de Rosnay, P., Rozum, I., Vamborg, F.,
596 Villaume, S., and Thepaut, J. N.: The ERA5 global reanalysis, *Quarterly Journal of the Royal
597 Meteorological Society*, 146, 1999-2049, 10.1002/qj.3803, 2020.

598 Huang, X., Ding, K., Liu, J. Y., Wang, Z. L., Tang, R., Xue, L., Wang, H. K., Zhang, Q., Tan, Z. M., Fu,
599 C. B., Davis, S. J., Andreae, M. O., and Ding, A. J.: Smoke-weather interaction affects extreme wildfires
600 in diverse coastal regions, *Science*, 379, 457-461, 10.1126/science.add9843, 2023.

601 Huffman, G. J., Bolvin, D. T., Nelkin, E. J., and Tan, J.: Integrated Multi-satellitE Retrievals for GPM
602 (IMERG) technical documentation, Nasa/Gsfc Code, 612, 2019, 2015.

603 Huffman, G. J., Bolvin, D. T., Braithwaite, D., Hsu, K.-L., Joyce, R. J., Kidd, C., Nelkin, E. J., Sorooshian,
604 S., Stocker, E. F., and Tan, J.: Integrated multi-satellite retrievals for the global precipitation measurement
605 (GPM) mission (IMERG), Satellite Precipitation Measurement: Volume 1, 343-353, 2020.

606 Ichoku, C., Ellison, L. T., Willmot, K. E., Matsui, T., Dezfuli, A. K., Gatebe, C. K., Wang, J., Wilcox, E.
607 M., Lee, J., and Adegoke, J.: Biomass burning, land-cover change, and the hydrological cycle in Northern
608 sub-Saharan Africa, *Environmental Research Letters*, 11, 095005, 2016.

609 Jiang, Y. Q., Yang, X. Q., Liu, X. H., Qian, Y., Zhang, K., Wang, M. H., Li, F., Wang, Y., and Lu, Z.:
610 Impacts of Wildfire Aerosols on Global Energy Budget and Climate: The Role of Climate Feedbacks, *J
611 Climate*, 33, 3351-3366, 10.1175/Jcli-D-19-0572.1, 2020.

612 Jolly, W. M., Cochrane, M. A., Freeborn, P. H., Holden, Z. A., Brown, T. J., Williamson, G. J., and
613 Bowman, D. M. J. S.: Climate-induced variations in global wildfire danger from 1979 to 2013, *Nature
614 Communications*, 6, ARTN 753710.1038/ncomms8537, 2015.

615 Kanamitsu, M., Ebisuzaki, W., Woollen, J., Yang, S.-K., Hnilo, J., Fiorino, M., and Potter, G.: NCEP–DOE
616 AMIP-II Reanalysis (R-2), *B Am Meteorol Soc*, 83, 1631-1644, 2002.

617 Knorr, W., Dentener, F., Lamarque, J. F., Jiang, L. W., and Arneth, A.: Wildfire air pollution hazard during
618 the 21st century, *Atmos Chem Phys*, 17, 9223-9236, 10.5194/acp-17-9223-2017, 2017.

619 Koster, R. D., Darmenov, A. S., and da Silva, A. M.: The quick fire emissions dataset (QFED):
620 Documentation of versions 2.1, 2.2 and 2.4, 2015.

621 Kreidenweis, S. M., Remer, L. A., Bruintjes, R., and Dubovik, O.: Smoke aerosol from biomass burning in
622 Mexico: Hygroscopic smoke optical model, *Journal of Geophysical Research: Atmospheres*, 106, 4831-
623 4844, 2001.

624 Lee, Y. S., Collins, D. R., Li, R., Bowman, K. P., and Feingold, G.: Expected impact of an aged biomass
625 burning aerosol on cloud condensation nuclei and cloud droplet concentrations, *Journal of Geophysical
626 Research: Atmospheres*, 111, 2006.

627 Liu, Y. W., Zhang, K., Qian, Y., Wang, Y. H., Zou, Y. F., Song, Y. J., Wan, H., Liu, X. H., and Yang, X.
628 Q.: Investigation of short-term effective radiative forcing of fire aerosols over North America using nudged
629 hindcast ensembles, *Atmos Chem Phys*, 18, 31-47, 10.5194/acp-18-31-2018, 2018.

630 Lu, Z., Liu, X., Zhang, Z., Zhao, C., Meyer, K., Rajapakshe, C., Wu, C., Yang, Z., and Penner, J. E.:
631 Biomass smoke from southern Africa can significantly enhance the brightness of stratocumulus over the
632 southeastern Atlantic Ocean, *Proceedings of the National Academy of Science*, 201713703, 2018.

633 Magi, B., Rabin, S., Shevlakova, E., and Pacala, S.: Separating agricultural and non-agricultural fire
634 seasonality at regional scales, *Biogeosciences*, 9, 3003, 2012.

635 Marlon, J. R., Bartlein, P. J., Carcaillet, C., Gavin, D. G., Harrison, S. P., Higuera, P. E., Joos, F., Power,
636 M., and Prentice, I.: Climate and human influences on global biomass burning over the past two millennia,
637 *Nature Geoscience*, 1, 697-702, 2008.

638 Mouillot, F. and Field, C. B.: Fire history and the global carbon budget: a 1×1 fire history reconstruction
639 for the 20th century, *Global Change Biology*, 11, 398-420, 2005.

640 Page, S. E., Siegert, F., Rieley, J. O., Boehm, H. D. V., Jaya, A., and Limin, S.: The amount of carbon
641 released from peat and forest fires in Indonesia during 1997, *Nature*, 420, 61-65, 10.1038/nature01131,
642 2002.

643 Pechony, O. and Shindell, D.: Fire parameterization on a global scale, *Journal of Geophysical Research: Atmospheres*, 114, 2009.

645 Perdigon-Morales, J., Romero-Centeno, R., Barrett, B. S., and Ordonez, P.: Intraseasonal Variability of 646 Summer Precipitation in Mexico: MJO Influence on the Midsummer Drought, *J Climate*, 32, 2313-2327, 647 10.1175/Jcli-D-18-0425.1, 2019.

648 Power, M. J., Marlon, J., Ortiz, N., Bartlein, P. J., Harrison, S. P., Mayle, F. E., Ballouche, A., Bradshaw, 649 R. H., Carcaillet, C., and Cordova, C.: Changes in fire regimes since the Last Glacial Maximum: an 650 assessment based on a global synthesis and analysis of charcoal data, *Climate dynamics*, 30, 887-907, 2008.

651 Prasad, V. K., Badarinath, K., and Eaturu, A.: Biophysical and anthropogenic controls of forest fires in the 652 Deccan Plateau, India, *Journal of Environmental Management*, 86, 1-13, 2008.

653 Randerson, J., Chen, Y., Werf, G., Rogers, B., and Morton, D.: Global burned area and biomass burning 654 emissions from small fires, *Journal of Geophysical Research: Biogeosciences*, 117, 2012.

655 Rogers, C. M. and Bowman, K. P.: Transport of smoke from the Central American fires of 1998, *Journal 656 of Geophysical Research: Atmospheres*, 106, 28357-28368, 2001.

657 **Running, S., Q. Mu, M. Zhao. : MODIS/Terra Gross Primary Productivity 8-Day L4 Global 500m SIN 658 Grid V061,distributed by NASA EOSDIS Land Processes Distributed Active Archive Center, 659 <https://doi.org/10.5067/MODIS/MOD17A2H.061>. Accessed 2023-12, 2021.**

660 Tosca, M., Randerson, J., Zender, C., Flanner, M., and Rasch, P. J.: Do biomass burning aerosols intensify 661 drought in equatorial Asia during El Nino?, *Atmospheric Chemistry and Physics*, 10, 3515-3528, 2010.

662 Tosca, M. G., Randerson, J. T., and Zender, C. S.: Global impact of smoke aerosols from landscape fires 663 on climate and the Hadley circulation, *Atmos Chem Phys*, 13, 5227-5241, 10.5194/acp-13-5227-2013, 664 2013.

665 van Marle, M. J. E., Kloster, S., Magi, B. I., Marlon, J. R., Daniau, A. L., Field, R. D., Arneth, A., Forrest, 666 M., Hantson, S., Kehrwald, N. M., Knorr, W., Lasslop, G., Li, F., Mangeon, S., Yue, C., Kaiser, J. W., and 667 van der Werf, G. R.: Historic global biomass burning emissions for CMIP6 (BB4CMIP) based on merging 668 satellite observations with proxies and fire models (1750-2015), *Geosci Model Dev*, 10, 3329-3357, 669 10.5194/gmd-10-3329-2017, 2017.

670 Veira, A., Lasslop, G., and Kloster, S.: Wildfires in a warmer climate: Emission fluxes, emission heights, 671 and black carbon concentrations in 2090–2099, *Journal of Geophysical Research: Atmospheres*, 121, 3195- 672 3223, 2016.

673 Vermote, E.: NOAA CDR Program: NOAA Climate Data Record (CDR) of AVHRR Leaf Area Index 674 (LAI) and Fraction of Absorbed Photosynthetically Active Radiation (FAPAR), Version 5, Version, 5, 675 NOAA National Centers for Environmental Information. , 2019.

676 Voulgarakis, A. and Field, R. D.: Fire influences on atmospheric composition, air quality and climate, 677 *Current Pollution Reports*, 1, 70-81, 2015.

678 Winker, D. M., Tackett, J. L., Getzewich, B. J., Liu, Z., Vaughan, M. A., and Rogers, R. R.: The global 3- 679 D distribution of tropospheric aerosols as characterized by CALIOP, *Atmos Chem Phys*, 13, 3345-3361, 680 10.5194/acp-13-3345-2013, 2013.

681 Yokelson, R., Urbanski, S., Atlas, E., Toohey, D., Alvarado, E., Crounse, J., Wennberg, P., Fisher, M., 682 Wold, C., and Campos, T.: Emissions from forest fires near Mexico City, *Atmos. Chem. Phys*, 7, 5569- 683 5584, 2007.

684 Yokelson, R. J., Crounse, J., DeCarlo, P., Karl, T., Urbanski, S., Atlas, E., Campos, T., Shinozuka, Y., 685 Kasputin, V., and Clarke, A.: Emissions from biomass burning in the Yucatan, *Atmospheric Chemistry and 686 Physics*, 9, 5785, 2009.

687 Yue, S., Zhu, J., Chen, S., Xie, Q., Li, W., Li, L., Ren, H., Su, S., Li, P., and Ma, H.: Brown carbon from
688 biomass burning imposes strong circum-Arctic warming, *One Earth*, 5, 293-304, 2022.

689 Zhang, Y. W., Fan, J. W., Shrivastava, M., Homeyer, C. R., Wang, Y., and Seinfeld, J. H.: Notable impact
690 of wildfires in the western United States on weather hazards in the central United States, *P Natl Acad Sci
691 USA*, 119, ARTN e220732911910.1073/pnas.2207329119, 2022.

692 Zhong, Q. R., Schutgens, N., van der Werf, G., van Noije, T., Tsigaridis, K., Bauer, S. E., Mielonen, T.,
693 Kirkevag, A., Seland, O., Kokkola, H., Checa-Garcia, R., Neubauer, D., Kipling, Z., Matsui, H., Ginoux,
694 P., Takemura, T., Le Sager, P., Remy, S., Bian, H. S., Chin, M., Zhang, K., Zhu, J. L., Tsyro, S. G., Curci,
695 G., Protonotariou, A., Johnson, B., Penner, J. E., Bellouin, N., Skeie, R. B., and Myhre, G.: Satellite-based
696 evaluation of AeroCom model bias in biomass burning regions, *Atmos Chem Phys*, 22, 11009-11032,
697 10.5194/acp-22-11009-2022, 2022.

698